Available online at www.sciencedirect.com
ScienceDirect
Trans. Nonferrous Met. Soc. China 34(2024) 3194−3207
Transactions of Nonferrous Metals Society of China
www.tnmsc.cn

High-throughput studies and machine learning for design of β titanium alloys with optimum properties

Wei-min CHEN[1], Jin-feng LING[2], Kewu BAI[3], Kai-hong ZHENG[1], Fu-xing YIN[1], Li-jun ZHANG[4], Yong DU[4]

1. Guangdong Provincial Key Laboratory of Metal Toughening Technology and Application, National Engineering Research Center of Powder Metallurgy of Titanium & Rare Metals, Institute of New Materials, Guangdong Academy of Sciences, Guangzhou 510650, China;
2. Institute of Advanced Wear & Corrosion Resistant and Functional Materials, Jinan University, Guangzhou 510632, China;
3. Institute of High Performance Computing, Agency for Science, Technology and Research, 138632, Singapore;
4. State Key Laboratory of Powder Metallurgy, Central South University, Changsha 410083, China

Received 29 March 2023; accepted 9 October 2023

Abstract: Based on experimental data, machine learning (ML) models for Young's modulus, hardness, and hot-working ability of Ti-based alloys were constructed. In the models, the interdiffusion and mechanical property data were high-throughput re-evaluated from composition variations and nanoindentation data of diffusion couples. Then, the Ti−(22±0.5)at.%Nb−(30±0.5)at.%Zr−(4±0.5)at.%Cr (TNZC) alloy with a single body-centered cubic (BCC) phase was screened in an interactive loop. The experimental results exhibited a relatively low Young's modulus of (58±4) GPa, high nanohardness of (3.4±0.2) GPa, high microhardness of HV (520±5), high compressive yield strength of (1220±18) MPa, large plastic strain greater than 30%, and superior dry- and wet-wear resistance. This work demonstrates that ML combined with high-throughput analytic approaches can offer a powerful tool to accelerate the design of multicomponent Ti alloys with desired properties. Moreover, it is indicated that TNZC alloy is an attractive candidate for biomedical applications.

Key words: high-throughput; machine learning; Ti-based alloys; diffusion couple; mechanical properties; wear behavior

1 Introduction

Metallic biomaterials have attracted rapidly increasing attention in recent decades due to good combination of strength and plasticity and have been widely used in biomedical applications, such as bone plates and dental roots [1−4]. Among them, the metallic implant materials including stainless steels, Co−Cr-based alloys, and α/β Ti−6Al−4V have certain biological toxicity for the clinical applications and may lead to other diseases [5−7]. The commercially pure (CP) Ti with the α phase has low hardness and bad wear resistance, greatly shortening its service life [8]. Moreover, the above clinical implants have a higher elastic modulus than bones or teeth, resulting in stress shielding phenomena, and further leading to aggravations, including bone instability and bone loss. Therefore, β Ti alloys with good biocompatibility, appropriate mechanical properties, and good corrosion resistance have been developed as alternative metallic implant materials [9−12]. Among them, Ti−Nb−Zr alloys with a suitable Young's modulus have attracted extensive attention [13−15]. Alloying elements, such as Cr, Hf, Mo, Sn, or Ta, are often

Corresponding author: Wei-min CHEN, Tel: +86-20-87716053, E-mail: chenweiming126@163.com
DOI: 10.1016/S1003-6326(24)66602-1

added to Ti alloys to provide thermodynamically more stable body-centered cubic (BCC) alloy and/or better mechanical properties [16−20]. The high-throughput approaches are thus urgently needed as the compositional space of the β Ti alloys is significantly enlarged.

The machine learning (ML) method, originally used for determining the structure−activity relationship of medicine and biological phenomena [21,22], is parallelly applied in exploring the structure−property relationships in material science in recent years [23−33]. The ML method has been used to predict the property data of arbitrary composition in the wide composition range of multicomponent Ti alloys, and then to screen the materials with exceptional property using a large number of experimental data to build the property databank [16,28]. Despite the growing use of ML models in designing the β Ti alloys, there are still drawbacks to its underlying design models. First, most ML-based material models have been focused on optimizing a single objective, mainly Young's modulus of Ti alloys, because of its importance in the stress shielding effect. Although the failure of Ti alloys utilized in the bio-applications frequently occurs through a synergistic combination of multiple properties, only a few multi-objective ML models have been used to explore the crucial properties of the Ti alloys. As far as we know, no multi-objective ML has been utilized to design the multicomponent Ti alloys with optimum properties, such as low Young's modulus, high hardness, high wear resistance, and good hot workability. Second, the physical and chemical properties of Ti alloys are often used as essential features of the ML models to improve the prediction and interpretation performance of the model. These models face difficulties in the forward and inverse design of multiple properties of multicomponent Ti alloys. In contrast, alloy compositions are often employed as the features, and common algorithms (i.e., the support vector machine and the Gaussian process) are used in the regression of the property data, which can be found in Refs. [26,28,31,34].

The ML application can accelerate the discovery of novel materials, but needs plenty of reliable data [35]. The data acquired by using traditional trial-and-error methods are limited in the vast composition space and huge amounts of research work are still needed. High-throughput measurements on the specimens with a relatively small volume are urgently developed for the composition-dependent property data to reduce the experimental cost and time. Nanoindentation conducted on the diffusion couple/multiple was proposed by ZHAO [36] and illustrated in the recent literature [37−39] to obtain a number of mechanical property data. Young's modulus and hardness can be obtained by reverse analysis algorithms from the nanoindentation data [34,40]. Since wear property is determined by the hardness and Young's modulus, the wear resistance of materials can be indirectly characterized by ratios of hardness to Young's modulus [41]. Moreover, very recently, a hot workability parameter defined by the ratio of the effective diffusion coefficient to the cube of Young's modulus has been utilized to qualitatively estimate the steady-state rate at intermediate temperatures [38,39]. The effective diffusion coefficient is obtained from the composition-dependent interdiffusion coefficients determined using a pragmatic numerical inverse method [42−44]. The above combinational method based on the diffusion couple, nanoindentation, and electron probe microanalysis (EPMA) techniques is a high-throughput analytic approach to determine the mechanical, diffusion, and wear properties. Therefore, multi-objective ML combined with high-throughput determination plays a very significant role in predicting the accurate property data for the multicomponent alloys with the desired mechanical, wear, and hot-working properties.

The ML-type databanks built using reliable and high-throughput data can be used to explore the Ti bio-alloys with optimum mechanical and wear properties from the vast composition space of three or more metallic elements. Young's modulus, hardness, and hot workability are the research objects in the interactive loop. First, the compositions with low Young's modulus are selected from the investigated compositions. Subsequently, the compositions with high hardness are picked from the selected compositions. The final compositions with high hot workability are found within the existing composition data. After the selection, the compositions with low Young's modulus, high hardness, and high hot workability can be found as potential Ti bio-alloys with excellent mechanical properties and superior wear resistance.

In this study, ML combined with high-throughput analytic approaches was used to establish the mechanical and diffusion property databanks of the BCC Ti−Nb−Zr− (Cr, Hf, Mo, Sn, and Ta) systems. Moreover, an interactive loop was presented to guide the rational design of the biomedical Ti alloys with the desired mechanical properties and superior wear resistance. First, experimental data on interdiffusion and mechanical properties of Ti−Nb−Zr−(Cr, Hf, Mo, Sn, and Ta) alloys [20,37−39] were re-evaluated by the pragmatic numerical inverse method and reverse analysis algorithms from the raw data such as composition profiles and nanoindentation information. Subsequently, the composition-dependent property databanks of Ti−Nb−Zr-based quaternary alloys were built by the ML method to provide Young's modulus, hardness, and hot workability parameters. Finally, novel Ti alloys with low Young's modulus, high hardness, and good hot workability parameter would be selected and verified by microstructure characterization and mechanical properties and wear behavior tests.

2 Theoretical method

ML method was utilized to predict the β Ti alloys with low modulus, high hardness (or yield stress), and good hot-workability. The reverse analysis algorithms [40] were used to extract Young's modulus and hardness from the load−displacement (L−D) curves of quaternary diffusion couples [20,37−39], while a pragmatic numerical inverse method was used to obtain the interdiffusion coefficients from the corresponding composition gradients [42]. And then, the composition-dependent Young's modulus, hardness, and hot workability parameters were conducted as property databanks of quaternary Ti alloys for training and testing data of ML. The composition was denoted as input variable, and the property data including Young's modulus, hardness, and hot workability parameter were denoted as response variables. In the calculations, cross-validation method was adopted to randomly divide the input data into training and testing data. Several models such as linear regression (LR), support vector regression (SVR), and Gaussian process regression (GPR) were employed to build the correlation between composition and property.

3 Experimental

3.1 Sample preparation and microstructure characterization

The Ti, Nb, Zr, and Cr slugs with a purity of more than 99.9 wt.% from ZhongNuo Advanced Material (Beijing) Technology Co., Ltd. (China) were used for the fabrication of the predicted Ti−22Nb−30Zr−4Cr (at.%) alloy by ML. To ensure compositional homogeneity, Ti−Nb−Zr−Cr alloy was flipped and remelted five times by arc melting under an Ar atmosphere using a non-consumable tungsten electrode (WKDHL−1, Opto-electronics Co., Ltd., Beijing, China), and then poured into a copper mold with a size of 10 mm × 10 mm × 50 mm. Several blocks sealed into vacuum tubes was annealed at (1273±2) K for 2 h in an ELF1106-type furnace (Carbolite Gero Co., Ltd., United Kingdom), and quenched with flowing water. In addition, Ti6Al4V and CP Ti from ZhongNuo Advanced Material (Beijing) Technology Co., Ltd. (China) were also used here for comparisons. The as-cast and solution-treated Ti−22Nb−30Zr−4Cr alloy, Ti6Al4V and CP Ti were denoted as AC-TNZC, ST-TNZC, TC4, and CP-Ti, respectively. The compositions were determined by the field emission EPMA equipped with a wavelength-dispersive spectrometer (WDS), and the phase constitutions of the above samples were characterized by X-ray diffraction (XRD, Ultima IV, Rigaku, Tokyo, Japan) with a Cu K_α radiation source (λ=0.1506 nm), a scanning step of 2 (°)/min, and a 2θ scan range of 20°−90° under an accelerating voltage of 40 kV and a current of 40 mA. The morphology and structure of the samples were examined by using optical microscope (DMT3000) and scanning electron microscope (SEM). The analysis of electron backscatter diffraction (EBSD) was conducted using thermal field emission scanning microscope (JSM−IT800). Before microstructural characterization, the samples were ground to remove surface contaminations and polished, followed by electropolishing with $HClO_4$, $CH_3(CH_2)_3OH$, and CH_3OH solutions at 35 V and −20 °C for 90 s to reveal the grain boundaries.

3.2 Mechanical property tests

The microhardness tests were performed in a

microhardness tester (HXD−1000TMC, Taiming Inc., Shanghai, China) with an indentation load of 200 g and dwell time of 15 s. At least 9 indentations were tested on each sample surface and the average values were taken to ensure the accuracy. The nanoindentation tests combined with reverse analysis algorithms were conducted by a nano-indenter (Keysight G200, Agilent Technology, USA) with an in-depth control (2000 nm) to obtain the Young's modulus and hardness. The measured mechanical property data were expressed as means± standard deviation (SD). Compressive tests were carried out on an INSTRON universal materials testing machine with a cross-head speed of 0.5 and 1 mm/min at room temperature, respectively. Square cylinder compression specimens were prepared according to the GB/T 7314 standard by considering the ratio of diameter to the length between 1.5 and 2. The average values of three measurements were considered for compressive property.

3.3 Wear property tests

The wear properties of the samples with the size of 10 mm × 10 mm × 5 mm were measured on a multi-functional tribometer (MFT−5000, Rtec instruments, Co., Ltd., USA) under the ambient atmospheric and simulated body fluid (SBF, pH= 7.4) solution conditions, respectively. SBF solution was composed of KCl (0.225 g/L), $K_2HPO_4·3H_2O$ (0.231 g/L), $MgCl_2·6H_2O$ (0.311 g/L), $CaCl_2$ (0.292 g/L), Na_2SO_4 (0.072 g/L), Tris (6.118 g/L), NaCl (8.035 g/L), $NaHCO_3$ (0.355 g/L), and 1.0 mol/L HCl (39 mL) [45]. Zirconia ceramic balls with a diameter of 5 mm were used as the couple-pair. The parameters used in this experiment were a normal force of 2 N, a sliding time of 1 h and sliding frequency of 1 Hz. Before the wear test, the samples were mechanically ground to 5 μm by waterproof silicon carbide sandpaper, and polished to a mirror-like surface with silica suspension for ensuring similar surface roughness. The coefficient of friction (COF) was recorded during the test. The wear rate was determined by the ratio of wear volume loss to sliding distance. The wear volume was calculated by two-dimensional (2D) curves of the wear mark multiplied by the total length of wear mark, which can be obtained from the three-dimensional (3D) wear morphology. And the sliding distance was equal to the product of sliding distance per second and sliding time (here, the sliding time was set to be 1 h). More than or equal to 3 sliding experiments were repeated for each sample. After that, the wear morphologies of samples were evaluated by using the SEM.

4 Results and discussion

4.1 High-throughput determinations of experimental data from diffusion couples

One of the fundamental assumptions of the current ML method is the availability of large and uniformly sampled (or balanced) training data. Unfortunately, the balanced data in the vast composition space of β Ti alloys are exceedingly rare. To overcome this issue, the experimental information reported in the previous investigations [20,37−39], including the *L*−*D* curves and composition versus distance profiles of the Ti−Nb−Zr−(Cr, Hf, Mo, Sn, and Ta) diffusion couples, was utilized to provide the mechanical and diffusion properties to establish the property databanks. It is noted that Ti−Nb−Zr−(Cr, Hf, Mo, Sn, and Ta) diffusion couples within the single β phase were used to produce the experimental data of β Ti alloys. The reverse analysis algorithms [40] were used to reassess Young's modulus and hardness of quaternary Ti−Nb−Zr−(Cr, Hf, Mo, Sn, and Ta) alloys with a fixed Poisson's ratio of 0.3 from the corresponding *L*−*D* curves. It was found that one diffusion couple could provide dozens of indentations with different compositions. Thus, 1290 sets of mechanical properties could be obtained from a series of Ti−Nb−Zr-based diffusion couples. Moreover, the pragmatic numerical inverse method [42] was used to determine the quaternary interdiffusion coefficients from the composition distribution profiles along the diffusion direction. The main interdiffusion coefficients of the solute element with the largest atomic radius were then obtained as effective diffusion coefficients for the compositions corresponding to the aforementioned indentations to calculate the hot workability parameter. Figure 1 shows the variations of Young's modulus, hardness, and hot workability parameters for the quaternary Ti−Nb−Zr−(Cr, Hf, Mo, Sn, and Ta) alloys. It is seen that Young's modulus, hardness, and hot workability parameter were closely related to the alloy composition. Solute elements, such as Hf, Nb, Sn, Ta, and Zr, can increase the equilibrium

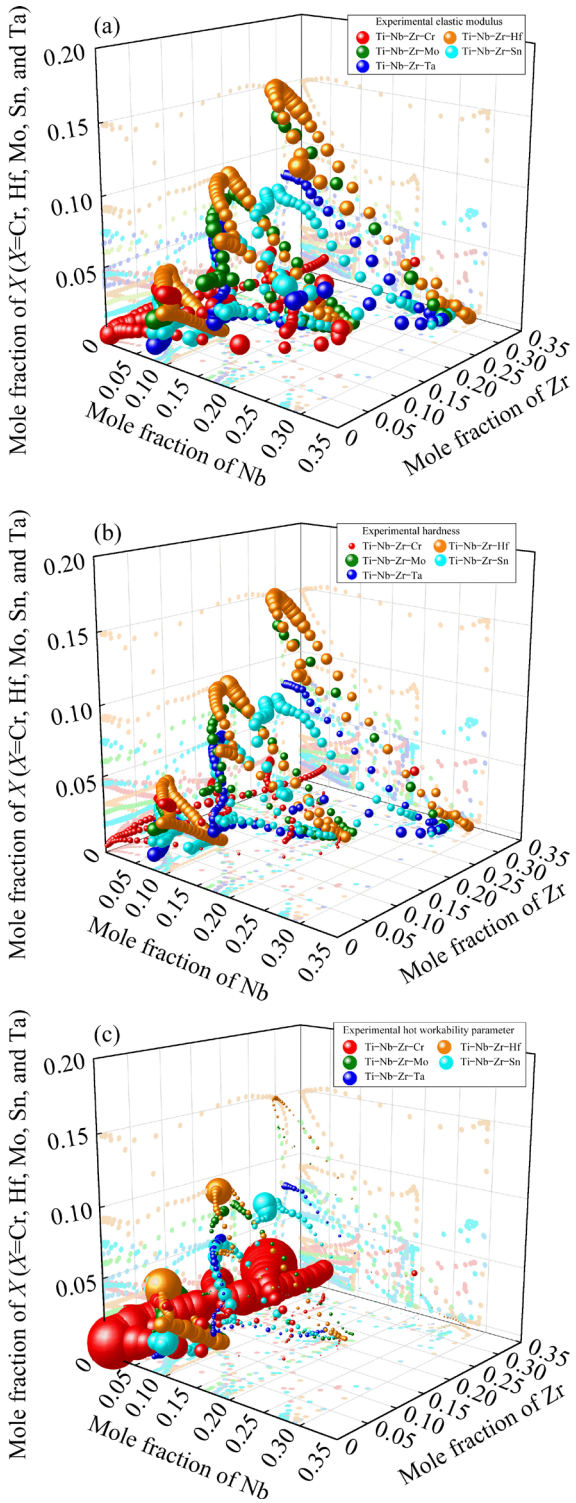

Fig. 1 Experimental elastic modulus (a), hardness (b), and hot workability parameter (c) of quaternary Ti−Nb−Zr−(Cr, Hf, Mo, Sn, and Ta) alloys re-evaluated from literature data [21−24]

lattice constant of Ti alloys, thus decreasing their Young's moduli. Due to solid solution strengthening, the hardness of Ti alloys increases with increasing the solute element contents. The high Young's modulus, low effective diffusion coefficient, or both may cause the low hot workability parameter. The low diffusion coefficients of Nb, Hf, Sn, and Ta can reduce the hot workability parameter of Ti alloys. In contrast, the high diffusion coefficient of Zr has a positive effect on improving the hot workability. The composition-dependent Young's modulus, hardness, and hot workability parameters were used as the input data in the subsequent ML modeling.

The property databanks of Ti-rich Ti−Nb−Zr−(Cr, Hf, Mo, Sn, and Ta) systems were built using the ML, and the Young's modulus, hardness, and hot workability parameter were predicted. The root mean squared errors (RMSEs) of LR, SVR, and GPR models are presented in Fig. 2. The RMSE of the GPR model for Young's modulus, hardness, and hot workability parameter was the lowest, and the LR model had a higher RMSE than the SVR model. This indicates that the GPR model is suitable for constructing ML property databanks. The possible reason may be the practical advantage of the GPR model providing uncertain estimations on the predictions for probabilistic modeling purposes. Moreover, the GPR model is a simple yet powerful tool for dealing with a large set of multi-variable sample data, which can also be easy to maintain and update the available sample data [46]. The GPR model results are illustrated in Fig. 2, and are compared with the experimental data obtained from the high-throughput technique. It is shown that the agreements between ML predictions and experimental data are excellent. The presently established property databanks were then used by interactive loops to select the Ti alloys with exceptional properties. Because more than 30 at.% of the Nb solute element can be necessary to stabilize the β phase of Ti alloys [47] and Nb is a more efficient BCC stabilizer in the Ti matrix than Zr, the Nb and Zr contents should be within the composition range of 15−35 at.% in calculations, respectively. In the first loop, for all the composition points with a composition interval of 0.5 at.% (the maximum content of the third solute element was 10 at.%), the alloys should have Young's modulus of lower than 63 GPa (about 55% of Young's modulus of CP-Ti [48] and TC4 [49]). Then, the alloys were utilized in the second selection. For the retained alloys, the ones with a hardness of higher than 3.2 GPa (slightly higher than hardness

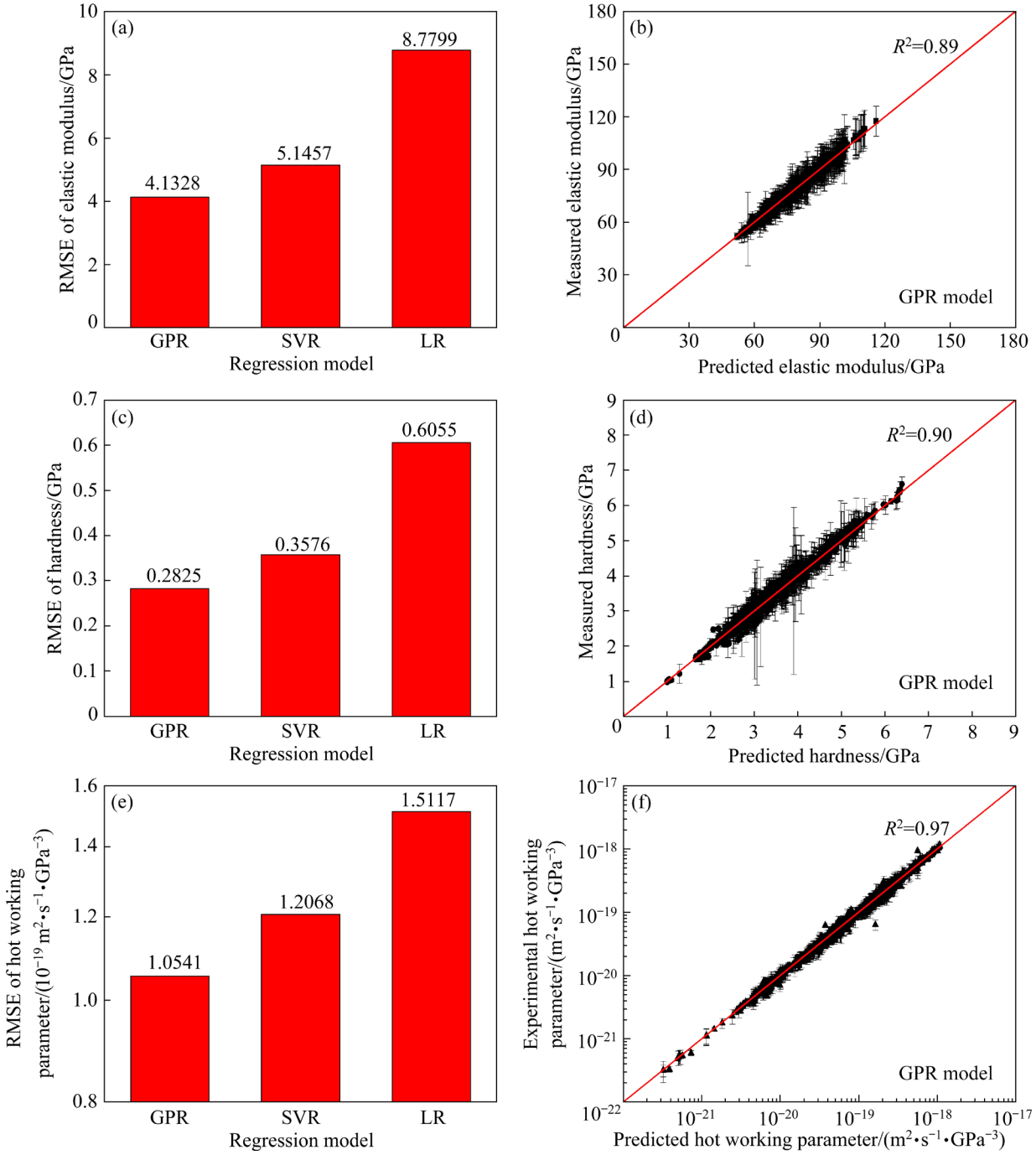

Fig. 2 Root mean squared errors (RMSEs) of three regression models for Young's modulus (a), hardness (c), and hot workability parameter (e) of Ti-rich Ti−Nb−Zr−(Cr, Hf, Mo, Sn, and Ta) alloys, and comparisons between experimental Young's modulus (b), hardness (d), and hot workability parameter (f) and predicted data by using ML method

of CP-Ti [48]) were conserved in the second loop. The last loop achieved the targets with the hot workability parameter greater than 1×10^{-19} m^2·s^{-1}·GPa^{-3} (slightly higher than the parameter of the TC4 alloy [38]). Figure 3 shows the screening process based on the ML-type property databanks of Ti-rich Ti−Nb−Zr−(Cr, Hf, Mo, Sn, and Ta) systems. It can be seen that many alloys have a low Young's modulus, but limited alloys can have excellent mechanical and process-ability properties. After the selection, compositions with exceptional properties were predicted. Therefore, final composition of Ti−(22±0.5)at.%Nb−(30±0.5)at.%Zr−(4±0.5)at.%Cr could be obtained, with the predicted Young's modulus of 62.56 GPa, the hardness of 3.23 GPa, and the hot workability

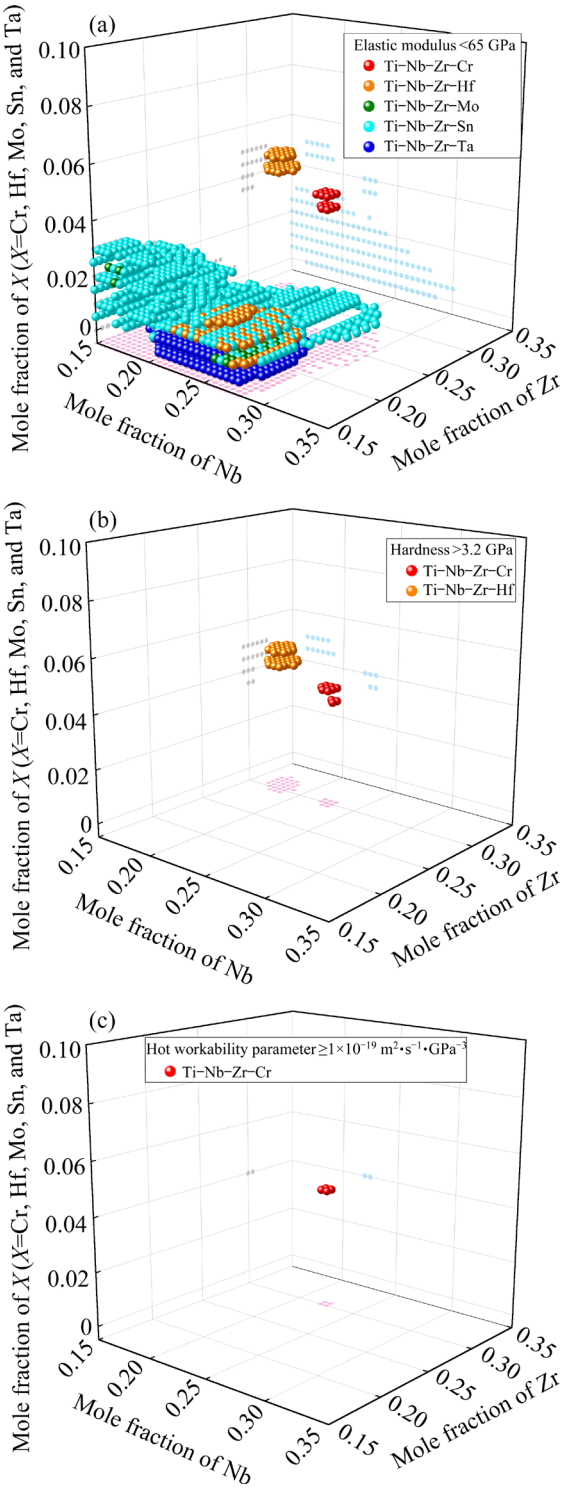

Fig. 3 Alloy compositions satisfying requirements of low Young's modulus (a), high hardness (b), and high hot workability parameter (c) in Ti-rich Ti–Nb–Zr–(Cr, Hf, Mo, Sn, and Ta) systems

parameter of 1.04×10^{-19} m$^2\cdot$s$^{-1}\cdot$GPa^{-3}. This target alloy predicted from the ML was very close to the alloy selected using Young's modulus databank [20]. This indicates that both the ML and CALculation of PHAse Diagrams (CALPHAD) methods could provide similar predicted results for the same requirements. It is noted that the CALPHAD-type property databank always suffers from the fundamental model parameters used as a kind of input data. For example, the property data of BCC Zr have an important effect on the databank reliability, but they are not accurately measured or computed due to the $\alpha\rightarrow\beta$ phase transition. Thus, the accurate property data of pure elements and binary and ternary alloys are urgently needed for the quaternary system, significantly restricting the establishment of CALPHAD-type databanks. ML approach allows the computation of the property data directly from the existing data and has no special input data. The compositions of quaternary alloys were independent variables in the present input data and were used to predict the properties in the quaternary Ti–Nb–Zr-based systems. Thermodynamic and phenomenological parameters such as melting temperature, mixing enthalpy, Pauling electronegativity difference, and valence electron concentration can be converted from the composition information combined with the end-members of pure metals [32]. Then, they can be utilized as features to discover the relation with the properties. Once the intrinsic relationships between these key features and properties are established, the properties of quinary and higher-order element alloys may be well predicted. The recently proposed framework could accelerate the exploration of multicomponent alloys with exceptional properties by combining high-throughput calculations and the active learning method in Ref. [50]. Thus, the active learning method based on high-throughput determinations and high-throughput calculations can be very helpful in constructing the desired databank and rapidly screen the target alloys. It is noted that both the ML and CALPHAD methods can predict better results from more experimental data. Quaternary Ti–(22±0.5)at.%Nb–(30±0.5)at.%Zr–(4±0.5)at.%Cr alloy was selected from the present ML predictions.

4.2 Microstructure and mechanical properties

Figure 4(a) shows the XRD patterns of AC-TNZC, ST-TNZC, TC4, and CP-Ti. It can be seen that the TC4 alloy was composed of α and β phases and CP-Ti had a single α phase. Importantly, the main peaks of the β phase at 2θ of 38.7°, 55.9°,

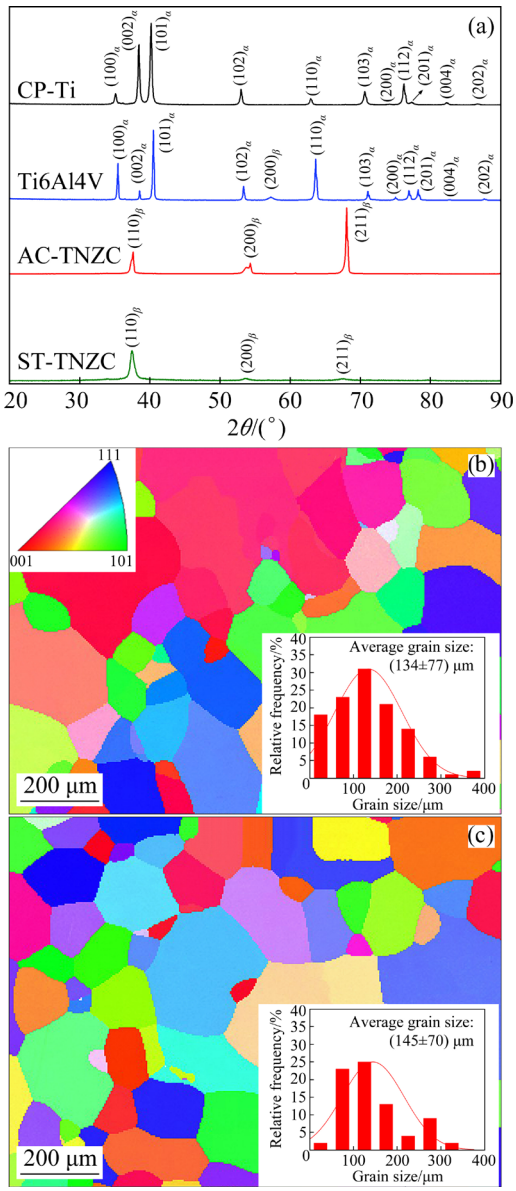

Fig. 4 XRD patterns of CP Ti and Ti alloys (a), and EBSD maps of AC-TNZC (b) and ST-TNZC (c) alloys

70.1°, and 80.1° were detected in the AC- and ST-TNZC alloys, corresponding to $(110)_\beta$, $(200)_\beta$, $(211)_\beta$ and $(220)_\beta$, respectively. It is worth noting that, compared with the β phase in the TC4 alloy, the positions of the β phase peaks related to the TNZC alloys shifted as a whole toward a lower angle. This is attributed to the increase in the lattice constants with increasingly larger Zr and Nb atoms. The EBSD maps of TNZC alloys in the as-cast and solution treated states are presented in Figs. 4(b, c). It is shown that both two specimens were composed of equiaxed grains, and the distributions of their grain orientation were random.

The microhardness, Young's modulus, and hardness of the pure Ti and Ti alloys were determined from the micro- and nanoindentation tests, as listed in Table 1. It can be seen that the TNZC alloy exhibited the highest hardness value of about HV 519−535, and the microhardness of the TNZC alloy was nearly triple that of the CP-Ti and twice that of the TC4 alloy. The results indicated that the microhardness of Ti alloys with the β phase was higher than that of Ti alloys with the α phase, which agrees well with the results in Ref. [51]. The Young's modulus and hardness of CP-Ti and TC4 alloy obtained from the nanoindentation agreed with the reference data (Young's modulus and hardness of CP-Ti were within the range of 108−131 GPa and 1.9−3.8 GPa [48], respectively, and Young's modulus and hardness of TC4 alloy were (121±3) GPa and (5±0.1) GPa [49], respectively). The measured data of the TNZC alloy were in excellent agreement with the ML results (62.56 GPa for Young's modulus and 3.23 GPa for hardness). Moreover, the compressive stress−strain curves of the pure Ti and Ti alloys at room temperature are shown in Fig. 5. It can be seen that the TNZC alloy and CP-Ti were not fractured when the compressive strain was up to 50%, exhibiting their good plasticity. The 0.2% proof compressive yield strengths ($\sigma_{0.2}$) of AC-TNZC, ST-TNZC, TC4, and CP-Ti were (1202.2±13.8), (1220.3±17.9), (891.1±35.1), and (340.1±16.4) MPa, respectively. The $\sigma_{0.2}$ values of AC- and ST-TNZC were very close, and the result of the TNZC alloy was about 35% and 2.5 times that of TC4 and CP-Ti, respectively.

Table 1 Microhardness, Young's modulus, and hardness of CP-Ti and Ti alloys measured from micro- and nano-indentation tests

Sample	Microhardness (HV)	Hardness/GPa	Young's modulus/GPa
CP-Ti	166.9±20.6	1.9±0.2	123±9
TC4	308.8±18.7	3.1±0.2	115±5
AC-TNZC	535.6±22.5	3.5±0.2	63±2
ST-TNZC	519.6±15.5	3.4±0.2	58±4

4.3 Wear property

Figures 6(a, b) display the wear volume and wear rate of CP-Ti and Ti alloys under both dry and wet sliding conditions. It can be intuitively seen that the dry wear volume loss or wear rate of the AC-TNZC alloy was only half that of the TC4 alloy

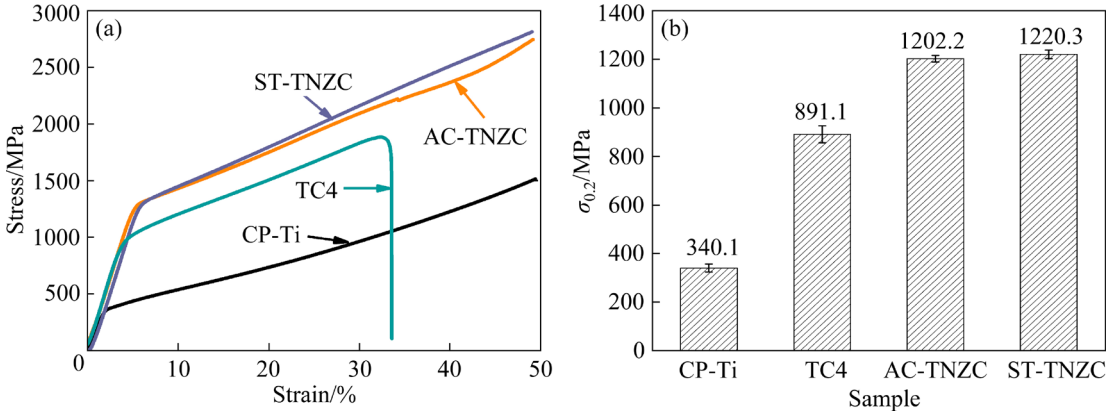

Fig. 5 Compression stress−strain curves (a) and corresponding compressive yield strengths (b) of CP-Ti and Ti alloys

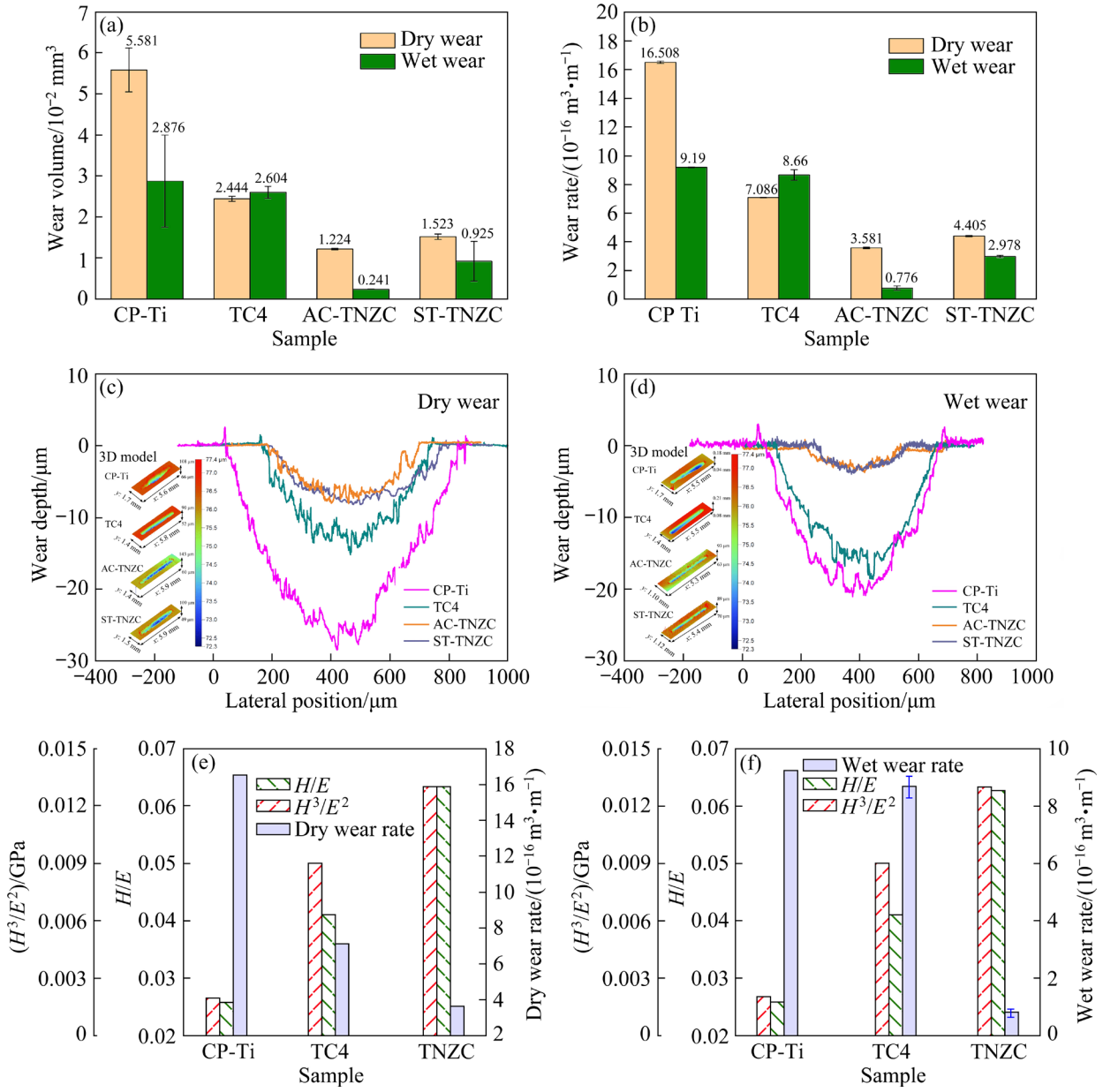

Fig. 6 Wear volume (a) and wear rate (b) of CP-Ti and Ti alloys under dry sliding and wet sliding in SBF solution, two-dimension wear track profiles of CP-Ti and Ti alloys under dry (c) and wet (d) sliding, and relationships between dry (e) or wet (f) wear rates and ratios of hardness to Young's modulus of CP-Ti and Ti alloys

and slightly lower than the value of ST-TNZC alloy, while CP Ti had the highest wear volume loss and wear rate. This indicates that the TNZC alloy exhibited the highest wear resistance under the dry sliding condition. Similar results were obtained for the wet condition. The 2D wear track profiles of CP-Ti and Ti alloys are also shown in Figs. 6(c, d). It is worth noting that the TNZC alloy had the shallowest and narrowest 2D wear track profiles under both dry and wet reciprocating friction environments. The lower the wear volume of the samples was, the shallower the wear profiles were. Intriguingly, the wear track profiles of the TC4 alloy under the sliding in the SBF solution tended to be deeper than those in the dry sliding condition. The ratios of hardness (H) to Young's modulus (E) (i.e., H/E and H^3/E^2) of CP-Ti and Ti alloys are plotted in Figs. 6(e, f), along with the corresponding wear rates. There was an inverse correlation between the wear rates and hardness-to-elastic modulus ratios. Although the hardness of the TC4 alloy was close to that of the TNZC alloy, the high Young's modulus led to the high wear rate of the TC4 alloy. In addition, the wear rate of the TC4 alloy during sliding in the SBF solution was larger than that during the dry sliding, which may be caused by the interplay between wear and corrosion. The H/E and H^3/E^2 ratios can be utilized to reflect the wear property of materials, consistent with the descriptions in Refs. [14,41]. Therefore, this qualitative method lays a foundation for selecting bio-alloys with excellent wear resistance.

The COF curves for CP-Ti and Ti alloys during the sliding are illustrated in Figs. 7(a, b). It is shown that the COF value under wet sliding in the SBF solution had a larger fluctuation than that under dry sliding. This is attributed to the lubrication effect of the SBF solution. Moreover, the COFs for CP-Ti and Ti alloys are shown in Fig. 7(c). The results demonstrate that the COFs of CP-Ti and Ti alloys could be reduced due to the lubrication of the SBF solution. In addition, the COF value of the TNZC alloy was slightly higher than that of CP-Ti and TC4, indicating that CP-Ti and TC4 alloy had a better lubrication effect. Figure 8 shows the SEM morphologies of wear scars for CP-Ti and Ti alloys under both the dry and wet sliding. Typical wear features, including plowing grooves, microcracks, adhesion, and delamination could be found. After the solution treatment, the TNZC alloy had the

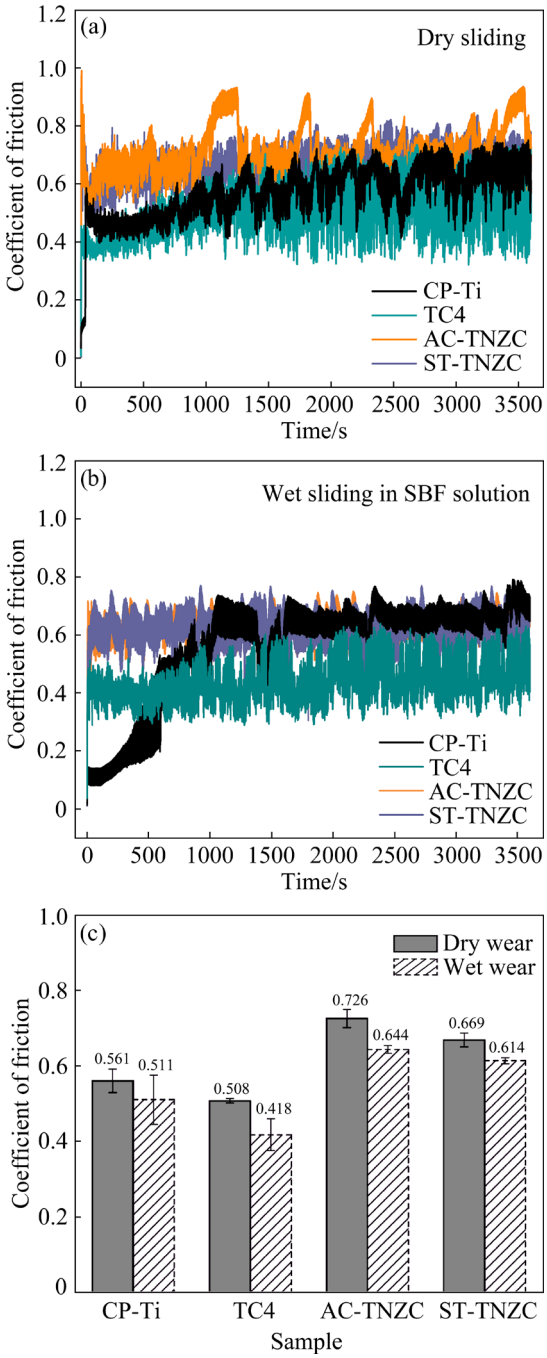

Fig. 7 Curves of COF for CP-Ti and Ti alloys during dry (a) and wet (b) sliding, and measured coefficients of friction for CP-Ti and Ti alloys (c)

shallowest plowing grooves and the least surface delamination, corresponding to the lowest wear volume loss and wear rate. This is caused by the low Young's modulus and relatively high hardness. Owing to the combination of wear and corrosion, the plowing grooves of TC4 got deeper, and its delamination was more significant under the wet wear condition.

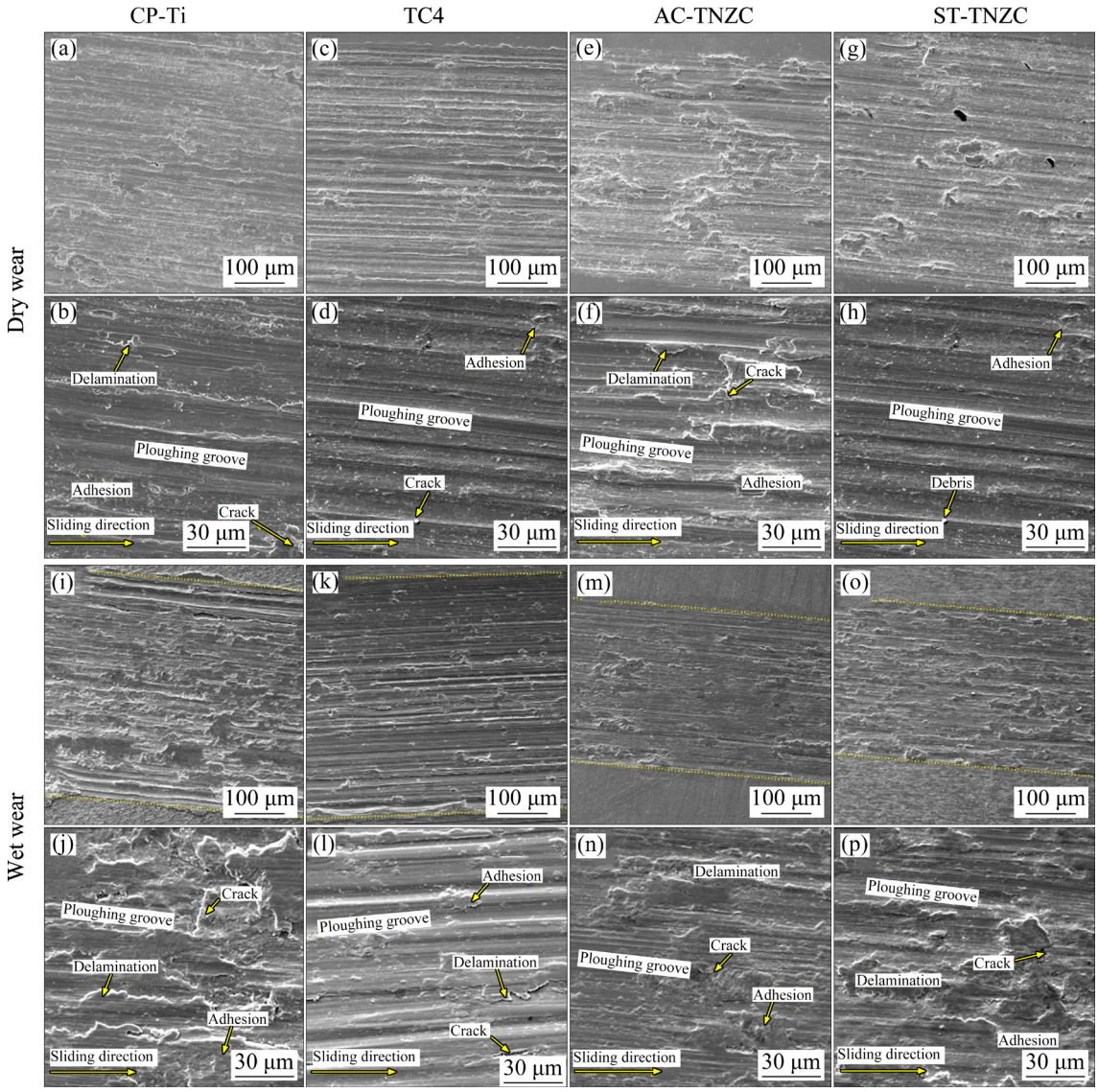

Fig. 8 SEM images of worn scar surfaces of CP-Ti and Ti alloys under dry and wet sliding conditions

5 Conclusions

(1) The property databanks of the Ti−Nb−Zr-based quaternary alloys were successfully established by using the ML method. A Ti−(22±0.5)at.%Nb−(30±0.5)at.%Zr−(4±0.5)at.%Cr (TNZC) alloy was selected from the built ML databanks. The predicted elastic modulus, hardness, and hot workability parameter of TNZC alloy were 62.56 GPa, 3.23 GPa, and 1.04×10^{-19} $m^2\cdot s^{-1}\cdot GPa^{-3}$, respectively.

(2) TNZC alloy had only β phase and equiaxed grains with random grain-orientation. A dendrite structure in the arc-melted TNZC alloy disappeared after solution annealing. TNZC alloy had an optimal combination of a relatively low Young's modulus of (57.5±4.1) GPa, high nanohardness of (3.4±0.2) GPa, high microhardness of HV (520±5), high compressive yield strength of (1220±18) MPa, and large plastic strain of greater than 30% according to nanoindentation, microhardness, and compression tests.

(3) TNZC alloy had a superior wear resistance under both dry and wet wear conditions to CP-Ti and TC4, and an inverse correlation between the wear rates and hardness-to-Young's modulus ratio was verified. The present results indicated that TNZC alloy had excellent comprehensive properties, which could be used as the candidate to replace traditionally CP-Ti and TC4 alloy in biomedical applications.

CRediT authorship contribution statement

Wei-min CHEN: Conceptualization, Investigation, Formal analysis, Visualization, Supervision, Writing − Original draft, Writing − Review & editing, Project administration, Funding acquisition; **Jin-feng LING:** Investigation, Visualization, Writing − Original draft, **Ke-wu BAI:** Investigation, Formal analysis, Writing − Review & editing; **Kai-hong ZHENG:** Formal analysis; **Fu-xing YIN:** Formal analysis; **Li-jun ZHANG:** Visualization; **Yong DU:** Writing − Review & editing.

Declaration of competing interest

The authors declare that they have no known competing financial interests or personal relationships that could have appeared to influence the work reported in this paper.

Data availability

The data and calculation codes that support the findings of this study are available from the corresponding author upon reasonable request.

Acknowledgments

The authors gratefully acknowledge the financial supports from the National Key Research and Development Program of China (No. 2022YFB3707501), the National Natural Science Foundation of China (No. 51701083), the GDAS Project of Science and Technology Development, China (No. 2022GDASZH-2022010107), and the Guangzhou Basic and Applied Basic Research Foundation, China (No. 202201010686). The authors thank Dr. Ren-gen DING for his technical assistance of EBSD measurements.

References

[1] ZHANG Ze-chuan, JIA Bo, YANG Hong-tao, HAN Yu, WU Qiang, DAI Ke-rong, ZHENG Yu-feng. Zn0.8Li0.1Sr−A biodegradable metal with high mechanical strength comparable to pure Ti for the treatment of osteoporotic bone fractures: In vitro and in vivo studies [J]. Biomaterials, 2021, 275: 120905.

[2] SUN Jiang, ZHANG Xin, SHI Zhang-zhi, GAO Xi-xian, LI Hui-yan, ZHAO Feng-yuan, WANG Jian-quan, WANG Lu-ning. Development of a high-strength Zn−Mn−Mg alloy for ligament reconstruction fixation [J]. Acta Biomaterialia, 2021, 119: 485−498.

[3] TU Hai-ling, ZHAO Hong-bin, FAN Yan-yan, ZHANG Qing-zhu. Recent developments in nonferrous metals and related materials for biomedical applications in China: A review [J]. Rare Metals, 2022, 41: 1410−1433.

[4] LI Qiang, HUANG Qi, LI Jun-jie, HE Qian-feng, NAKAI M, ZHANG Ke, NIINOMI M, YAMANAKA K, CHIBA A, NAKANO T. Microstructure and mechanical properties of Ti−Nb−Fe−Zr alloys with high strength and low elastic modulus [J]. Transactions of Nonferrous Metals Society of China, 2022, 32: 503−512.

[5] WALKER P R, LEBLANC J, SIKORSKA M. Effects of aluminum and other cations on the structure of brain and liver chromatin [J]. Biochemistry, 1989, 28: 3911−3915.

[6] PULEO D A, HUH W W. Acute toxicity of metal ions in cultures of osteogenic cells derived from bone marrow stromal cells [J]. Journal of Applied Biomaterials, 1995, 6: 109−116.

[7] GEURTSEN W. Biocompatibility of dental casting alloys [J]. Critical Reviews in Oral Biology and Medicine, 2002, 13: 71−84.

[8] HU Nan, XIE Ling-xia, LIAO Qing, GAO Ang, ZHENG Yan-yan, PAN Hao-bo, TONG Li-ping, YANG Da-zhi, GAO Nong, STARINK M J, CHU P K, WANG Huai-yu. A more defective substrate leads to a less defective passive layer: Enhancing the mechanical strength, corrosion resistance and anti-inflammatory response of the low-modulus Ti−45Nb alloy by grain refinement [J]. Acta Biomaterialia, 2021, 126: 524−536.

[9] TONG Xian, SUN Quan-xiang, ZHANG De-chuang, WANG Kun, DAI Yi-long, SHI Zi-mu, LI Yun-cang, DARGUSCH M, HUANG Sheng-bin, MA Jian-feng, WEN Cuie, LIN Ji-xing. Impact of scandium on mechanical properties, corrosion behavior, friction and wear performance, and cytotoxicity of a β-type Ti−24Nb−38Zr−2Mo alloy for orthopedic applications [J]. Acta Biomaterialia, 2021, 134: 791−803.

[10] KONG Wei-huan, COX S C, LU Yu, VILLAPUN V, XIAO Xiao-ling, MA Wen-you, LIU Min, ATTALLAH M M. The influence of zirconium content on the microstructure, mechanical properties, and biocompatibility of in-situ alloying Ti−Nb−Ta based β alloys processed by selective laser melting [J]. Materials Science and Engineering C, 2021, 131: 112486.

[11] AWAD A H, EL-HOFY H A, CHIBA A, GEPREEL M A H. Robust mechanical properties and corrosion resistance of new low-cost hot-forged and aged β-type Ti−14Mn−(x)Zr alloys [J]. Journal of Alloys and Compounds, 2022, 904: 164098.

[12] LIN Hao-qin, LING Jin-feng, CHEN Wei-min, WANG Yao, WU Xiao-ke, ZHANG Li-jun. High-throughput determination of mechanical and diffusion properties in the Ti−Ta−Fe alloys [J]. Transactions of Nonferrous Metals Society of China, 2022, 32: 3963−3972.

[13] SHI An-qi, CAI Dian-geng, HU Jia-li, ZHAO Xiao-tong, QIN Gao-wu, HAN Yong, ZHANG Er-lin. Development of a low elastic modulus and antibacterial Ti−13Nb−13Zr−5Cu titanium alloy by microstructure controlling [J]. Materials Science and Engineering C, 2021, 126: 112116.

[14] WEN Zhu-hao, LIN Hao-qin, CHEN Wei-min, BAI Ke-wu, ZHANG Li-jun. High-throughput exploration of the composition-dependent elasto-plastic and diffusion properties of refractory multi-element Ti−Nb−Zr−W alloys [J]. Transactions of Nonferrous Metals Society of China, 2023, 33: 2646−2659.

[15] WANG Wen-jie, YANG Kai-huai, WANG Qian-ting, DAI

Pin-qiang, FANG Hui, WU Fang-juan, GUO Qiao-hang, LIAW P K, HUA Neng-bin. Novel Ti−Zr−Hf−Nb−Fe refractory high-entropy alloys for potential biomedical applications [J]. Journal of Alloys and Compounds, 2022, 906: 164383.

[16] YANG Fei, LI Zhen, WANG Qing, JIANG Bei-bei, YAN Biao-jie, ZHANG Peng-cheng, XU Wei, DONG Chuang, LIAW P K. Cluster-formula-embedded machine learning for design of multicomponent β-Ti alloys with low Young's modulus [J]. NPJ Computational Materials, 2020, 6: 101.

[17] CHEN Shu-ming, MA Ze-jun, QIU Shi, ZHANG Lian-ji, ZHANG Shang-zhou, YANG Rui, HU Qing-miao. Phase decomposition and strengthening in HfNbTaTiZr high entropy alloy from first-principles calculations [J]. Acta Materialia, 2022, 225: 117582.

[18] SITI NUR HAZWANI M R, LIM L X, LOCKMAN Z, ZUHAILAWATI H. Fabrication of titanium-based alloys with bioactive surface oxide layer as biomedical implants: Opportunity and challenges [J]. Transactions of Nonferrous Metals Society of China, 2022, 32: 1−44.

[19] MARKER C, SHANG S L, ZHAO J C, LIU Z K. Elastic knowledge base of bcc Ti alloys from first-principles calculations and CALPHAD-based modeling [J]. Computational Materials Science, 2017, 140: 121−139.

[20] LING Jin-feng, CHEN Wei-min, SHENG Yin-ying, LI Wei, ZHANG Li-jun, DU Yong. A MGI-oriented investigation of the Young's modulus and its application to the development of a novel Ti−Nb−Zr−Cr bio-alloy [J]. Materials Science and Engineering C, 2020, 106: 110265.

[21] BOLLS G, PACE L D, FABROCINI F. A machine learning approach to computer-aided molecular design [J]. Journal of Computer-aided Molecular Design, 1991, 5: 617−628.

[22] MJOLSNESS E, DECOSTE D. Machine learning for science: State of the art and future prospects [J]. Science, 2001, 293: 2051−2055.

[23] PILANIA G, WANG Chen-chen, JIANG Xun, RAJASEKARAN S, RAMPRASAD R. Accelerating materials property predictions using machine learning [J]. Scientific Reports, 2013, 3: 2810.

[24] LIU Ruo-qian, KUMAR A, CHEN Zheng-zhang, AGRAWAL A, SUNDARARAGHAVAN V, CHOUDHARY A. A predictive machine learning approach for micro-structure optimization and materials design [J]. Scientific Reports, 2015, 5: 11551.

[25] RACCUGLIA P, ELBERT K C, ADLER P D F, FALK C, WENNY M B, MOLLOL A, ZELLER M, FRIEDLER S A, SCHRIER J, NORQUIST A J. Machine-learning-assisted materials discovery using failed experiments [J]. Nature, 2016, 533: 73−76.

[26] RAO Zi-yuan, TUNG P Y, XIE Rui-wen, WEI Ye, ZHANG Hong-bin, FERRARI A, KLAVER T P C, KÖRMANN F, SUKUMAR P T, SILVA A K, CHEN Yao, LI Zhi-ming, PONGE D, NEUGEBAUER J, GUTFLEISCH O, BAUER S, RAABE D. Machine learning-enabled high-entropy alloy discovery [J]. Science, 2022, 378: 78−85.

[27] TIAN Yu-sheng, ZHOU Wen-zhe, TAN Qing-biao, WU Ming-xu, QIAO Shen, ZHU Guo-liang, DONG An-ping, SHU Da, SUN Bao-de. A review of refractory high-entropy alloys [J]. Transactions of Nonferrous Metals Society of China, 2022, 32: 3487−3515.

[28] XIE Jian-xin, SU Yan-jing, XUE De-zhen, JIANG Xue, FU Hua-dong, HUANG Hai-you. Machine learning for materials research and development [J]. Acta Metallurgica Sinica, 2021, 57: 1343−1361.

[29] ZOU Cheng-xiong, LI Jin-shan, WANG William Yi, ZHANG Ying, LIN Deye, YUAN Rui-hao, WANG Xiao-dan, TANG Bin, WANG Jun, GAO Xing-yu, KOU Hong-chao, HUI Xi-dong, ZENG Xiao-qin, QIAN Ma, SONG Hai-feng, LIU Z K, XU Dong-sheng. Integrating data mining and machine learning to discover high-strength ductile titanium alloys [J]. Acta Materialia, 2021, 202: 211−221.

[30] QIAO Ling, LAI Zhong-hong, LIU Yong, BAO A, ZHU Jing-chuan. Modelling and prediction of hardness in multi-component alloys: A combined machine learning, first principles and experimental study [J]. Journal of Alloys and Compounds, 2021, 853: 156959.

[31] QIAO Ling, RAMANUJAN R V, ZHU Jing-chuan. Machine learning discovery of a new cobalt free multi-principal-element alloy with excellent mechanical properties [J]. Materials Science and Engineering A, 2022, 845: 143198.

[32] VAZQUEZ G, SINGH P, SAUCEDA D, COUPERTHWAITE R, BRITT N, YOUSSEF K, JOHNSON D D, ARRÓYAVE R. Efficient machine-learning model for fast assessment of elastic properties of high-entropy alloys [J]. Acta Materialia, 2022, 232: 117924.

[33] LIU Xiu-juan, XU Peng-cheng, ZHAO Juan-juan, LU Wen-cong, LI Min-jie, WANG Gang. Material machine learning for alloys: Applications, challenges and perspectives [J]. Journal of Alloys and Compounds, 2022, 921: 165984.

[34] WEN Zhu-hao, HU Yun-long, CHEN Wei-min, ZHANG Qiang, ZHANG Li-jun, DU Yong. High-throughput exploration of the composition-dependent elasto-plastic properties in Co−Ni−W system [J]. Journal of Alloys and Compounds, 2022, 896: 163061.

[35] HUANG E W, LEE W J, SINGH S S, KUMAR P, LEE C Y, LAM T N, CHIN H H, LIN B H, LIAW P K. Machine-learning and high-throughput studies for high-entropy materials [J]. Materials Science and Engineering R, 2022, 147: 100645.

[36] ZHAO J C. Combinatorial approaches as effective tools in the study of phase diagrams and composition–structure–property relationships [J]. Progress in Materials Science, 2006, 51: 557−631.

[37] LING Jin-feng, HUANG Dan-dan, BAI Ke-wu, LI Wei, YU Zhen-tao, CHEN Wei-min. High-throughput development and applications of the compositional mechanical property map of the β titanium alloys [J]. Journal of Materials Science & Technology, 2021, 71: 201−210.

[38] WEN Zhu-hao, WANG Yong-zhe, LING Jin-feng, CHEN Wei-min, ZHANG Li-jun, DU Yong. High-throughput determination of the composition-dependent mechanical and diffusion properties in β Ti−Nb−Zr−Hf refractory alloys [J]. Journal of Alloys and Compounds, 2021, 876: 160150.

[39] WEN Zhu-hao, WANG Yao, CHEN Wei-min, ZHANG Li-jun, DU Yong. Investigation of mechanical and diffusion properties in bcc Ti−Nb−Zr−Sn alloys via a high-throughput method [J]. Transactions of Nonferrous Metals Society of China, 2021, 31: 3405−3415.

[40] DAO M, CHOLLACOOP N, VLIET K J V, VENKATESH T A, SURESH S. Computational modeling of the forward and reverse problems in instrumented sharp indentation [J]. Acta Materialia, 2001, 49: 3899−3918.
[41] LEYLAND A, MATTHEWS A. On the significance of the *H*/*E* ratio in wear control: A nanocomposite coating approach to optimised tribological behaviour [J]. Wear, 2000, 246: 1−11.
[42] CHEN Wei-min, ZHANG Li-jun, DU Yong, TANG Cheng-ying, HUANG Bai-yun. A pragmatic method to determine the composition-dependent interdiffusivities in ternary systems by using a single diffusion couple [J]. Scripta Materialia, 2014, 90/91: 53−56.
[43] CHEN Wei-min, ZHONG Jing, ZHANG Li-jun. An augmented numerical inverse method for determining the composition-dependent interdiffusivities in alloy systems by using a single diffusion couple [J]. MRS Communication, 2016, 6: 295−300.
[44] ZHONG Jing, CHEN Li, ZHANG Li-jun. Automation of diffusion database development in multicomponent alloys from large number of experimental composition profiles [J]. NPJ Computational Materials, 2021, 7: 35.
[45] TAMILSELVI S, RAMAN V, RAJENDRAN N. Corrosion behaviour of Ti−6Al−7Nb and Ti−6Al−4V ELI alloys in the simulated body fluid solution by electrochemical impedance spectroscopy [J]. Electrochimica Acta 2006, 52: 839−846.
[46] KHATAMSAZ D, VELA B, SINGH P, JOHNSON D D, ALLAIRE D, ARRÓYAVE R. Multi-objective materials Bayesian optimization with active learning of design constraints: Design of ductile refractory multi-principal-element alloys [J]. Acta Materialia, 2022, 236: 118133.
[47] RAABE D, SANDER B, M. FRIÁK, MA D, NEUGEBAUER J. Theory-guided bottom-up design of *β*-titanium alloys as biomaterials based on first principles calculations: Theory and experiments [J]. Acta Materialia, 2007, 55: 4475−4487.
[48] ATAEE A, LI Y, WEN C. A comparative study on the nanoindentation behavior, wear resistance and in vitro biocompatibility of SLM manufactured CP-Ti and EBM manufactured Ti64 gyroid scaffolds [J]. Acta Biomaterialia, 2019, 97: 587−596.
[49] HYNOWSKA A, PELLICER E, FORNELL J, GONZÁLEZ S, STEENBERGE N, SURIÑACH S, GEBERT A, CALIN M, ECKERT J, BARÓ M D, SORT J. Nanostructured *β*-phase Ti−31.0Fe−9.0Sn and sub-μm structured Ti−39.3Nb−13.3Zr−10.7Ta alloys for biomedical applications: Micro-structure benefits on the mechanical and corrosion performances [J]. Materials Science and Engineering C, 2012, 32: 2418−2425.
[50] DING Zhi-gang, ZHOU Jun-jun, YANG Piao, SUN Hao-ran, REN Ji-chang, ZHAO Yong-hao, LIU Wei. Accelerated exploration of high-performance multi-principal element alloys: Data-driven high-throughput calculations and active learning method [J]. Materials Research Letters, 2023, 11: 670−677.
[51] LEE C M, JU C P, LIN J H C, Structure−property relationship of cast Ti−Nb alloys [J]. Journal of Oral Rehabilitation, 2002, 29: 314−322.

用于设计具有最佳性能 *β* 钛合金的高通量研究和机器学习

陈伟民[1]，零锦凤[2]，Kewu BAI[3]，郑开宏[1]，殷福星[1]，张利军[4]，杜 勇[4]

1. 广东省科学院新材料研究所，国家钛及稀有金属粉末冶金工程技术研究中心，
广东省金属强韧化技术与应用重点实验室，广州 510650；
2. 暨南大学 先进耐磨蚀及功能材料研究院，广州 510632；
3. Institute of High Performance Computing, Agency for Science, Technology and Research, 138632, Singapore;
4. 中南大学 粉末冶金国家重点实验室，长沙 410083

摘 要：基于实验数据构建了钛基合金杨氏模量、硬度和热加工能力的机器学习模型。首先，从扩散偶的成分变化和纳米压痕数据中重新高通量评估互扩散和力学性能数据。然后，通过所构建的模型在交互循环中筛选出一种具有单一 BCC 相的 Ti−(22±0.5)%Nb−(30±0.5)%Zr−(4±0.5)%Cr (摩尔分数)(TNZC)合金。并且，该合金具有相对较低的杨氏模量((58±4) GPa)、高纳米硬度((3.4±0.2) GPa)、高显微硬度(HV (520±5))、高压缩屈服强度((1220±18) MPa)、大于 30%的大塑性应变以及优异的干磨损和湿磨损性能。结果表明，机器学习与高通量分析方法相结合可以作为一个强大的工具来加速设计具有优异性能的多元钛合金，同时也表明 TNZC 合金是生物医学应用中一种具有吸引力的候选材料。

关键词：高通量；机器学习；Ti 基合金；扩散偶；力学性能；磨损行为

(Edited by Bing YANG)